Dalton Transactions

ROYAL SOCIETY OF CHEMISTRY

PAPER

View Article Online
View Journal | View Issue



Cite this: *Dalton Trans.*, 2021, **50**, 2824

# A side-on Mn(III)–peroxo supported by a non-heme pentadentate $N_3Py_2$ ligand: synthesis, characterization and reactivity studies†

Dattaprasad D. Narulkar,[a,b] Azaj Ansari,[c] Anil Kumar Vardhaman,[d] Sarvesh S. Harmalkar,[a] Giribabu Lingamallu,[d] Vishal M. Dhavale,[e] Muniyandi Sankaralingam,[f] Sandip Das,[g] Pankaj Kumar[g] and Sunder N. Dhuri *[a]

A mononuclear manganese(III)–peroxo complex $[Mn^{III}(N_3Py_2)(O_2)]^+$ (**1a**) bearing a non-heme *N,N′*-dimethyl-*N*-(2-(methyl(pyridin-2-ylmethyl)amino)ethyl)-*N′*-(pyridin-2-ylmethyl)ethane-1,2-diamine ($N_3Py_2$) ligand was synthesized by the reaction of $[Mn(N_3Py_2)(H_2O)](ClO_4)_2$ (**1**) with hydrogen peroxide and triethylamine in $CH_3CN$ at 25 °C. The reactivity of **1a** in aldehyde deformylation using 2-phenyl propionaldehyde (2-PPA) was studied and the reaction kinetics was monitored by UV-visible spectroscopy. A kinetic isotope effect (KIE) = 1.7 was obtained in the reaction of **1a** with 2-PPA and α-[$D_1$]-PPA, suggesting nucleophilic character of **1a**. The activation parameters $\Delta H^{\ddagger}$ and $\Delta S^{\ddagger}$ were determined using the Eyring plot while $E_a$ was obtained from the Arrhenius equation by performing the reaction between 288 and 303 K. Hammett constants ($\sigma_p$) of *para*-substituted benzaldehydes *p*-X-Ph-CHO (X = Cl, F, H, and Me) were linear with a slope ($\rho$) = 3.0. Computational study suggested that the *side-on* structure of **1a** is more favored over the *end-on* structure and facilitates the reactivity of **1a**.

Received 27th October 2020,
Accepted 6th January 2021

DOI: 10.1039/d0dt03706k

rsc.li/dalton



## Introduction

Metal-dioxygen compounds are key intermediates formed during the dioxygen activation by various metal-containing enzymes.[1] In the 3d metal series, manganese plays a vital role in the active sites of several metalloenzymes, offering different oxidation states in redox reactions.[2] The manganese–peroxo intermediates have been detected as the reactive species in several enzymes like manganese superoxide dismutase (Mn-SOD),[3] manganese ribonucleotide reductase,[4] manganese homoprotocatechuate 2,3-dioxygenase (Mn-HPCD),[5] and oxygen-evolving complexes of photosystem II.[6] The manganese–peroxo adduct in Mn-SOD is the only structurally characterized intermediate in biological systems where the peroxide binds to the manganese by *side-on* binding mode instead of the *end-on* way.[7] Many manganese(III)–peroxo compounds bearing flexible and rigid ligand environments have been now reported and characterized by either spectroscopic methods or by X-ray crystallography (Scheme 1, ESI Table S1†).[8–13] The first

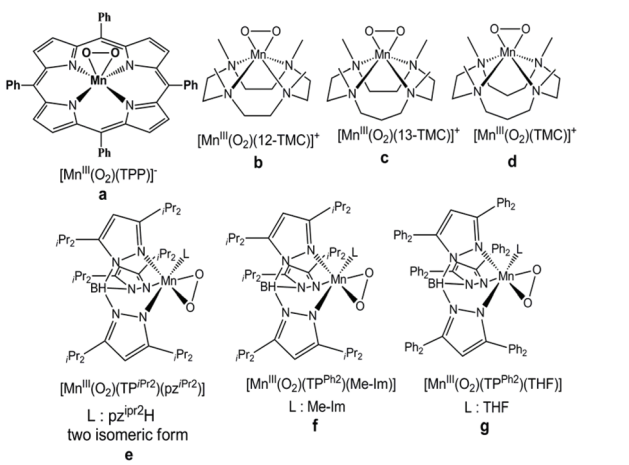


**Scheme 1** Structurally characterized Mn(III)-$O_2^{2-}$ intermediates.[13]

[a]*School of Chemical Sciences, Goa University, Goa-403206, India. E-mail: sndhuri@unigoa.ac.in; Tel: +918669609172*
[b]*Department of Chemistry, Dnyanprassarak Mandal's College and Research Centre, Assagao, Goa-403507, India*
[c]*Department of Chemistry, Central University of Haryana, Mahendergarh-123031, Haryana, India*
[d]*Polymers & Functional Materials Division, CSIR-Indian Institute of Chemical Technology, Uppal Road, Tarnaka, Hyderabad-500007, India*
[e]*CSIR-Central Electrochemical Research Institute, CSIR Madras Complex, Taramani, Chennai-600 113, India*
[f]*Bioinspired & Biomimetic Inorganic Chemistry Lab, Department of Chemistry, National Institute of Technology Calicut, Kozhikode, Kerala 673601, India*
[g]*Indian Institute of Science Education and Research (IISER), Tirupati-517507, India*
†Electronic supplementary information (ESI) available. See DOI: 10.1039/d0dt03706k

crystal structure of a *side-on* manganese(III)–peroxo species supported by a heme ligand tetraphenylporphyrin (TPP) was $[Mn^{III}(O_2)(TPP)]^-$ (structure a, Scheme 1).[9] The structural characterization and reactivity of Mn(III)–peroxo species bearing non-heme tetramethylated cyclam ligands namely, 12-TMC, 13-TMC, and 14-TMC were for the first time reported by Nam and co-workers (structures b–d, Scheme 1).[13a,b,c,15c] The structures of manganese(III)–peroxo species of trispyrazolyl based ligands such as (hydrotris(3,5-diisopropylpyrazol-1-yl)borate ($Tp^{ipr2}$) and tris(3,5-diphenylpyrazol)hydroborate ($Tp^{Ph2}$) are also investigated (structures e–g, Scheme 1).[10] Studies on a large number of Mn–peroxo intermediates have provided in-depth knowledge of their molecular and electronic structures and such intrinsic properties have been correlated with the reactivity of active sites of manganese-based enzymes.[8] The manganese containing enzymes usually react with oxidants like dioxygen, superoxides, or peroxides to form Mn-peroxide intermediates.[11] Several of the reported Mn(III)–peroxo species were prepared by reacting a Mn(II)-precursor compound with potassium superoxide,[9,12] hydrogen peroxide,[10] hydrogen peroxide in the presence of a mild base,[12c–e,13] or $O_2^{\bullet-}$ generated by electrochemical methods[14] or $O_2$[15] (see ESI Table S1†). It has been well documented that in the Mn–$O_2^{2-}$ species structure, the peroxo anion can exist in two binding modes *viz side-on* ($\eta^2$) or *end-on* ($\eta^1$).[8–13] The Mn(III)–peroxo intermediates bearing tetradentate ligands bind to Mn(III) in a *side-on* ($\eta^2$) peroxo species fashion,[8] while on the other hand, both *side-on* ($\eta^2$) and *end-on* ($\eta^1$) coordination modes are observed in Mn(III)–peroxo species bearing pentadentate ligands.[13c,e,13f,h–j] Nam and co-workers have well demonstrated the conversion of a *side-on* Mn(III)–peroxo species to *end-on* peroxo bearing a tetradentate TMC ligand on the addition of axial ligands at the fifth coordination site.[13c] However, the computational studies have shown that Mn(III)–peroxo species with pentadentate $N_5$ ligands ($mL_5^2$ and $imL_5^2$, N4Py, and Pro3Py) with a bispidine backbone can exist in only *side-on* ($\eta^2$) binding mode (Scheme 2).[13e,f,13h–j]

Apart from these two coordination modes (*side-on* ($\eta^2$) or *end-on* ($\eta^1$)), the formation of bis(μ-oxo)dimanganese (III, IV) wherein pentadentate ligands $N_4$py and dpaq are bound to Mn in an unusual tetradentate manner is also reported.[16]

The reactivity study of Mn(III)–peroxo species in the deformylation of aldehydes is well documented[13a–e] and in these reactions, Mn(III)–$O_2^{2-}$ species have nucleophilic character. Interestingly, in recent reports, it was shown that the deformylation of aldehydes by a Mn(III)–$O_2^{2-}$ species initially occurs *via* H-atom abstraction at the α-position to the –C(H)=O group in an electrophilic manner instead of nucleophilic attack on the carbonyl group of aldehyde.[13f,g,i] Since there are only a few reports on the electrophilic nature of an electron-rich manganese–peroxo species, it is important to investigate more such reactions using different ligands that stabilize manganese–peroxo intermediates. Influenced by the dichotomic reactivity of Mn(III)–peroxo intermediates (nucleophilic or electrophilic) proposed by the Nam and Sastri groups, herein we report the synthesis, characterization and reactivity studies of a new manganese(III)–peroxo stabilized by a non-heme pentadentate ligand *N*,*N*′-dimethyl-*N*-(2-(methyl(pyridin-2-ylmethyl)-amino) ethyl)-*N*′-(pyridin-2-ylmethyl-)ethane-1,2-diamine ($N_3Py_2$) at room temperature. Our literature studies show that very few peroxo intermediates are kinetically stable at room temperature, and others are spectroscopically detected at low temperatures (Table S1†).[10,13b,f] Many high valent metal–oxygen intermediates of pentadentate ligands similar to our ligand $N_3Py_2$ are stable at room temperature.[16a,17]

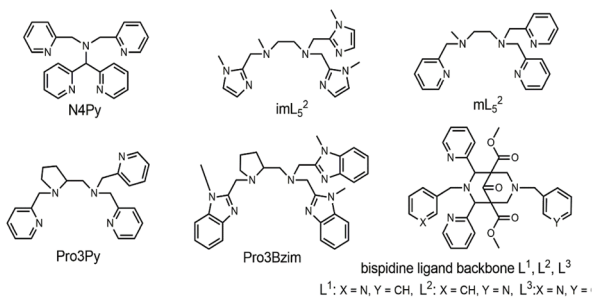


Scheme 2 List of $N_5$ pentadentate ligand supported Mn(III) peroxo structures.

## Experimental

### Materials and methods

All solid chemicals used in this work were purchased and used as received without recrystallization. The solvents were dried and distilled under a $N_2$ atmosphere before their use. $N_3Py_2$ and $[Mn(N_3Py_2)(H_2O)](ClO_4)_2$ (**1**) were prepared according to our recent report.[18,19] The deuterated 2-phenyl propionaldehyde was synthesized with a slight modification of the literature method.[20] A dry powder of sodium hydride (0.3 g) was taken in DMSO-$d_6$ maintained under an Ar atmosphere, and then the temperature was lowered to 0 °C. 2-Phenyl propionaldehyde (2-PPA) (1.335 mL) was then slowly added (this is an exothermic reaction and hence precautions are required), and the temperature of the reaction mixture was then slowly increased to 25 °C. The solution was kept under stirring for 8 h and then neutralized with $D_2O$, followed by extraction with ethyl acetate. Purity of >99% deuteration in the product was confirmed by $^1$H NMR spectroscopy (ESI, Fig. S1†). UV-visible spectra and kinetic data were collected on an Agilent diode array 8453 UV-visible spectrophotometer equipped with a circulating water bath. Electrospray ionization mass spectra (ESI-MS) of **1** and **1a** were recorded on an Agilent mass spectrometer (6200 series TOF/6500 series Q-TOF B.08.00), by infusing samples directly into the source using a manual method. $^1$HNMR spectra were measured with a Bruker model Ascend 400 FT-NMR spectrometer. The electron paramagnetic resonance (EPR) spectra were recorded using an X-band Bruker EMX-plus spectrometer equipped with a dual-mode cavity (ER 4116DM). Low temperatures were attained by using an Oxford Instruments ESR900 liquid He quartz cryostat with an Oxford Instruments ITC503 temperature and gas flow controller. The

experimental parameters for EPR spectra were as follows: microwave frequency = 9.648 GHz, microwave power = 1.0 mW, modulation amplitude = 10 G, gain = $1 \times 10^4$, modulation frequency = 100 kHz, time constant = 40.96 ms, conversion time = 85.00 ms and measurement temperature = 77 K. The product analysis was performed using a Shimadzu GC 2014 gas chromatograph equipped an HP capillary column (30 m × 0.25 mm × 2.5 μM) using an FID detector. The nitrogen gas was used as a carrier gas. The retention time and peak areas of the products were compared with those of authentic samples using decane as an internal standard.

### Computational techniques

All the geometry optimization was performed using Gaussian 09, a program suite.[21] In a similar work, several functionals such as B3LYP, B3LYP-D, wB97XD, B97D, M06-2X, OLYP, TPPSh, and MP2 were employed and B3LYP, B3LYP-D2, and wB97XD were advocated to correctly predict the spin ground state of the reactant and intermediates compared to experimental data.[22] Our calculations were restricted with two functionals, B3LYP and a dispersion corrected functional B3LYP-D2, for the geometry optimization of the Mn(III)–peroxo species **1a**.[23] Here, two different basis sets, LanL2DZ for Mn[24] and a 6-31G basis set, were used for the C, H, N, and O atoms.[25] The optimized geometries were then used to perform single-point energy calculations using a TZVP[26] basis set on all atoms. The quoted DFT energies are B3LYP-D2 solvation, including free-energy corrections with a TZVP basis set at a temperature of 298.15 K. The optimized geometries were verified by animating frequencies by using Chemcraft software. The solvation energies were computed at the B3LYP-D level by using a polarizable continuum model (PCM) with acetonitrile as a solvent.

### Synthesis of $[Mn(N_3Py_2)(H_2O)](ClO_4)_2$ (1)

Compound **1** was prepared according to our recent work.[18] $N_3Py_2$ (0.452 g, 1.38 mmol) in $CH_3CN$ (2 mL) was added to Mn $(ClO_4)_2{\cdot}6H_2O$ (0.5 g, 1.38 mmol) (2 mL $CH_3CN$) at RT under a $N_2$ atmosphere. The reaction mixture upon stirring for 12 h resulted in a brown solution. Addition of diethyl ether afforded a white-buff powder which on work-up gave yield = 0.68 (82%). Calc. for $C_{19}H_{31}N_5Cl_2O_9Mn$: C, 38.08; H, 4.91; N, 11.69%. Found C, 38.19; H, 4.91; N, 11.59%. IR (KBr, $cm^{-1}$): 3412 $\nu$(O–H); 1093, 621 $\nu(ClO_4)$. Magnetic moment, $\mu_{eff}$ = 5.97 BM. ESI-MS: $m/z$ = 191.18 (Calc. $m/z$ = 191.21): $[Mn(N_3Py_2)]^{2+}$ and $m/z$ = 481.08 (Calc. $m/z$ = 481.86): $[Mn(N_3Py_2)(ClO_4)]^+$.

### Generation of a Mn(III)–peroxo intermediate (1a)

A light purple manganese(III)–peroxo complex $[Mn(N_3Py_2)(O_2)]^+$ (**1a**) was generated by reacting Mn(II)-complex **1** (1 mM, 2 mL $CH_3CN$) with 10 equiv. of $H_2O_2$ (30% v/v) and 5 equiv. of triethylamine (TEA) at 25 °C. The formation of **1a** and its stability were analyzed by monitoring the spectral changes of the resulting solution with a UV-visible spectrophotometer. $\lambda_{max}$, $CH_3CN$/nm ($\varepsilon$/L $mol^{-1}$ $cm^{-1}$): 572(254), 412(120); magnetic moment, $\mu_{eff}$ = 2.91 BM, ESI-MS: $m/z$ = 414.17 (Calc. 414.17) for $[Mn(N_3Py_2)(^{16}O_2)]^+$ and $m/z$ = 418.17 (Calc. 418.17) for $[Mn(N_3Py_2)(^{18}O_2)]^+$.

### Reactivity studies of 1a

The reactivity of $[Mn(N_3Py_2)(^{16}O_2)]^+$ **1a** was investigated in deformylation of aldehydes such as 2-phenylpropionaldehyde (2-PPA) and cyclohexanecarboxyaldehyde (CCA). The reactions were performed in a 1 cm quartz cuvette and the kinetics of the reactions were followed by monitoring the decay of the 572 nm band of **1a** using a UV-visible spectrophotometer. Rate constants were determined under pseudo-first-order conditions (*i.e.*, [substrate]/[**1a**] > 10), by fitting the changes in the absorbance of the decay of the peak at 572 nm.

## Results and discussion

### Generation and characterization of 1a

The formation of $[Mn(N_3Py_2)(^{16}O_2)]^+$ **1a** intermediate in $CH_3CN$ was monitored by UV-visible spectroscopy (Fig. 1a). The UV-Vis spectrum of **1** in $CH_3CN$ exhibits bands only in the

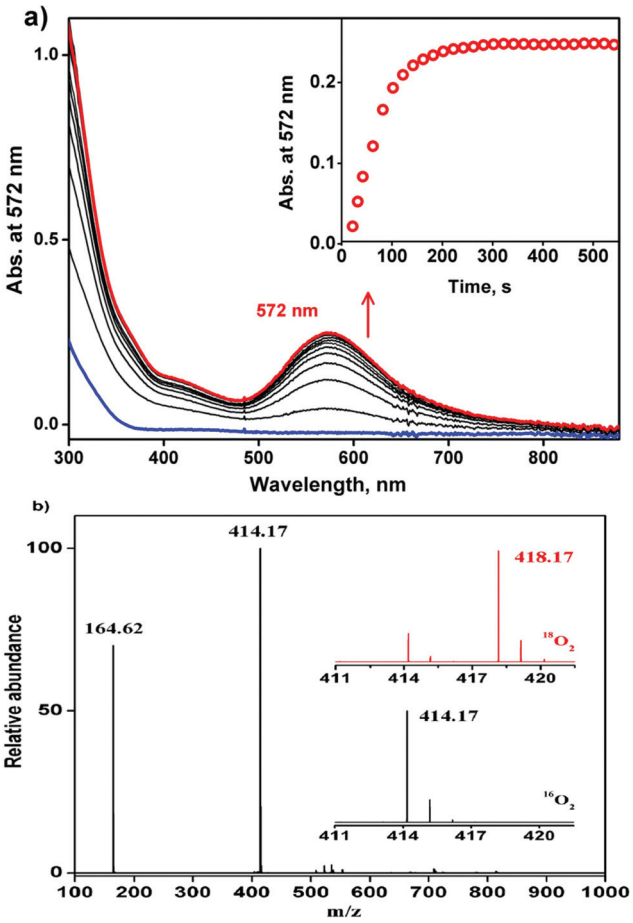


Fig. 1 (a) UV-visible spectral changes after the addition of 10 equiv. $H_2O_2$ in the presence of 5 eq. of TEA at 15 °C. The inset shows a time trace monitored at 572. (b) ESI-MS spectrum of **1a** recorded in $CH_3CN$ showing a mass peak at $m/z$ = 414.17 corresponding to $[Mn(N_3Py_2)(^{16}O_2)]^+$ species. The insets show the observed distribution patterns which correspond to the $[Mn(N_3Py_2)(^{16}O_2)]^+$ **1a** in black and $[Mn(N_3Py_2)(^{18}O_2)]^+$ in red. A peak $m/z$ = 164.62 corresponds to $[N_3Py_2H_2]^{2+}$.

UV region which are associated with intra-ligand transitions. The absorption spectrum of **1** in $CH_3CN$ does not show any band in the visible region,[18] which is the typical characteristic feature of high spin Mn(II) centers due to spin forbidden d–d transitions as observed in similar Mn(II) complexes.[27] On addition of 10 equiv. of $H_2O_2$ to the 1 mM solution of **1** in $CH_3CN$ in the presence of 5 equiv. of triethylamine (TEA) at 25 °C, the formation of a purple-colored intermediate (**1a**) was observed (ESI, Fig. S2†) with the appearance of a new band at 572 nm (254 ε/L $mol^{-1}$ $cm^{-1}$) and a shoulder peak at 412 nm (120 ε/L $mol^{-1}$ $cm^{-1}$) (Fig. 1a). The intermediate (**1a**) was stable for a sufficient time which allowed us to characterize and perform the reactions. The species (**1a**) was characterized by ESI-MS (Fig. 1b) and EPR studies (ESI, Fig. S3†). The ESI-MS of **1a** in $CH_3CN$ shows a peak at $m/z$ = 414.17 whose mass and isotopic distribution pattern corresponded to $[Mn(N_3Py_2)(O_2)]^+$ species (Calc. $m/z$ = 414.17). When $H_2{}^{18}O_2$ was used in the generation of **1a**, the peak due to Mn-$^{16}O_2$ shifted by two units to $m/z$ = 418.17. Unlike the EPR spectrum of **1** which showed six-line hyperfine signals (ESI, Fig. S3a†),[18] the X-band EPR spectrum of **1a** was devoid of any active signals, suggesting the EPR silent nature of **1a** (ESI, Fig. S3b†). These EPR data thus suggest that the Mn in **1a** is Mn(III) with a $d^4$ electron configuration.[13c] Furthermore, we have determined the magnetic moment of **1a**, using Evans' method,[28] and found it to be 2.91 BM (ESI, Fig. S4b†), in agreement with our assumption of a low spin $Mn^{3+}$ complex compared to high spin Mn(II) (ESI, Fig. S4a†). The ESI-MS, EPR and Evans method characterization results unambiguously support the formation of Mn(III)–peroxo intermediate **1a**. On confirming the formula of Mn(III)–peroxo species, the binding mode of **1a** was elucidated by using computational study (*vide infra*).

### Reactivity of 1a in aldehyde deformylation

The reactivity of **1a** was investigated by using different substrates. The electrophilic character of **1a** was initially tested in the oxidation of triphenylphosphine ($PPh_3$), thioanisole ($PhSCH_3$), cyclohexene and xanthene. However, we did not observe any spectral changes upon the addition of these substrates to the $CH_3CN$ solution of **1a** and the band at 572 nm remained the same. The product analysis of these reactions did not show the formation of any oxygenated products. This indicated to us that **1a** does not show electrophilic character in the above oxidation reactions. This is also in agreement with the peroxo species of other first-row transition metals reported earlier.[29] The reactivity of **1a** was then investigated in aldehyde deformylation as the precedent study of first-row transition metal–peroxo species showed the reactivity of Mn(III)–peroxo species with aldehydes. Upon addition of 10 equiv. of 2-PPA to the solution of **1a**, the UV-visible band at 572 nm decayed with a pseudo-first-order rate constant, $k_{obs}$ = 1.6 × $10^{-3}$ $s^{-1}$, and showed the isosbestic points at 501 and 778 nm (Fig. 2a). Upon increasing the concentration of 2-PPA, the pseudo-first-order rate constants increased proportionally, allowing us to determine a second-order rate constant ($k_2$) of 1.6 × $10^{-1}$ $M^{-1}$ $S^{-1}$ for the reaction at 25 °C (Fig. 2b).

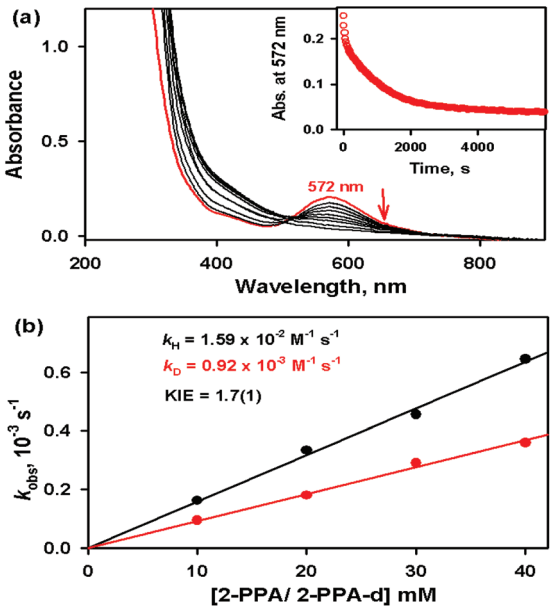


Fig. 2 (a) UV-visible spectral changes of **1a** (1 mM) upon addition of 10 equiv. of 2-PPA in acetonitrile. The inset shows the time course of the reaction monitored at 572 nm. (b) A plot of $k_{obs}$ against the concentration of 2-PPA and 2-PPA-*d* to determine the second-order rate constant.

The product analysis of the reaction mixture by the gas chromatographic (GC) method revealed acetophenone as the predominant product (88% (±2)) based on **1a** [29b,c] (Scheme 3). We have also investigated the reactivity of cyclohexanecarboxaldehyde (CCA) with **1a**; however, this reaction was very fast to determine kinetic data using a UV-Vis spectrometer. The product analysis of the final reaction mixture gave cyclohexene in quantitative yields (75% (±4)) based on the amount of **1a** used.[13b,c,29b,c] The activation parameters for the aldehyde deformylation reaction of 2-PPA were obtained from the Eyring plot to give $\Delta H^{\ddagger}$ and $\Delta S^{\ddagger}$ by determining pseudo-first-order rate constants from 288 to 303 K (Fig. 3a). The rates of reactions were dependent on the temperature, and a linear Eyring plot was obtained to give the activation parameters of $\Delta H^{\ddagger}$ = 42 (±2) kJ $mol^{-1}$ and $\Delta S^{\ddagger}$ = −139 (±3) J $mol^{-1}$ $K^{-1}$. The activation energy ($E_a$) = 42 (±1) kJ $mol^{-1}$ was obtained from the Arrhenius equation from the plot of ln $K_{obs}$ *versus* 1/$T$ (ESI, Fig. S5†).

It is reported that the proposed mechanism of aldehyde deformylation by metal–peroxo species involves a nucleophilic attack of peroxo species on the carbonyl group of an aldehyde forming peroxyhemiacetal intermediate.[13b,c,29] The O–O bond homolytic cleavage of this intermediate then yielded deformy-

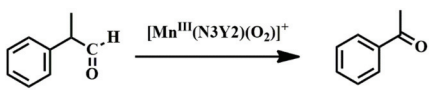


Scheme 3 Upon deformylation of 2-PPA, acetophenone is obtained as the major product.

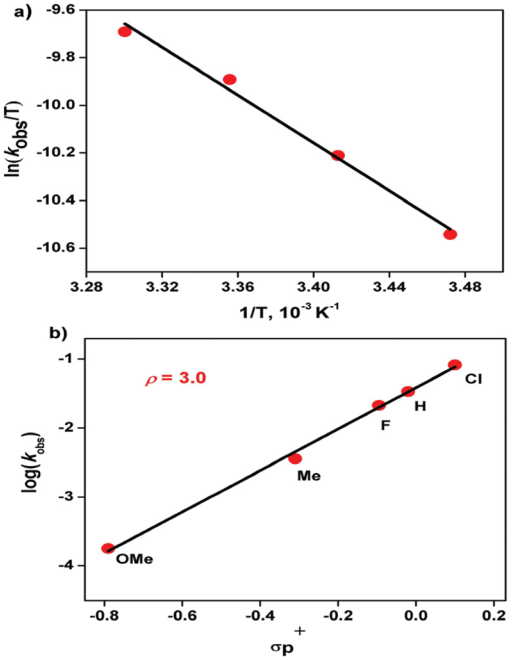


Fig. 3 (a) Plot of ln ($K_{obs}/T$) against 1/$T$ to determine the activation parameters for the reaction of **1a** and 2-PPA. (b) Hammett plot for the oxidation of *para*-substituted benzaldehydes p-X-Ph-CHO (X = Cl, F, H, and Me) by **1a** in $CH_3CN$ at 25 °C.

lated products.[29c] The ferric-peroxo porphyrin intermediate in cytochrome P450 progesterone 17α-hydroxylase-17,20-lyase (CYP 45017α) is reported to attack the carbonyl of progesterone, leading to the formation of androstenedione and acetate.[30] Very recently, Sastri and co-workers have demonstrated that the deformylation of an aldehyde such as 2-PPA by a nonheme Mn(III)–peroxo complex occurs *via* initial H-atom abstraction.[13f] Such an electrophilic abstraction was supported based on evidence such as the observation of a large kinetic isotope effect (KIE = 5.4) compared to KIE = 1 for the reaction of Mn(III)–peroxo with 2-PPA/α-[$D_1$]-PPA and computational studies.[13f,g,13i] They also reported that Mn(III)–peroxo species showed no reactivity with 2-methyl-2-phenyl propionaldehyde, which lacks α-hydrogen atoms. In the present, when we performed the reaction of **1a** with α-[$D_1$]-PPA, we obtained a second-order rate constant ($k_2$) of $9.3 \times 10^{-2}$ $M^{-1}$ $S^{-1}$, giving us KIE = 1.7 (Fig. 2b), and this value is slightly higher than the expected KIE = 1 for the nucleophilic reactions.[31] A slight increase in the value of KIE in our work could be attributed to the presence of a water molecule in the reaction mixture which is generated through the release from the parent compound $[Mn(N_3Py_2)(H_2O)]^{2+}$ **1** on addition of $H_2O_2$. Such a wet reaction in the presence of a trace amount of water is earlier reported by Tolman and coworkers.[32] Thus in comparison with the previous study, which showed a high kinetic effect (KIE = 5.4) for the deformylation of 2-PPA *via* initial H-atom abstraction, in our work we propose that the mechanism could still proceed *via* nucleophilic pathway as reported in several other 3d metal (III)–peroxo intermediates.[13b,e,29b,c,33] Further to support our notion of nucleophilicity of **1a**, we measured the reactivity of **1a** with different *para*-substituted benzaldehydes, *p*-X-Ph-CHO (where X = Cl, F, H, Me, and OMe) substrates. Our results suggest that the electron withdrawing *para*-substituents on the benzaldehyde react at a faster rate with **1a** compared to the electron donating *para*-substituted aldehydes, following the reactivity trend Cl > F > H > Me > OMe. The plot of log $k_{obs}$ *versus* Hammett constants ($\sigma_p^+$) was found to be linear, giving a slope ($\rho$) = 3.0 (Fig. 3b). These data thus provide additional evidence for the nucleophilic reactivity of **1a** with 2-PPA. Certain properties of ligands such as steric properties can affect the nucleophilic reactivity of Mn(III)–$O_2^{2-}$.[34] In our case we feel that the flexible ligand $N_3Py_2$ may be tangling around the Mn(III)–$O_2^{2-}$, making the initial H-atom abstraction process more difficult, thus following the nucleophilic pathway. To gain more understanding of the mechanism of deformylation of aldehydes and influence of ligand structures on reactivity, our efforts are underway to prepare new ligands which can stabilize M(III)–$O_2^{2-}$ species at room temperature.

## Computational studies

The experimental characterization gave a formula of **1a** as $[Mn(N_3Py_2)(\eta^2\text{-}O_2)]^+$. However, two isomeric structures for **1a** are possible, *end-on* $[Mn(N_3Py_2)(\eta^1\text{-}O_2)]^+$ (**1a$^1$**) and *side-on* $[Mn(N_3Py_2)(\eta^2\text{-}O_2)]^+$ (**1a$^2$**) (Scheme 4). To gain further insight into the stability of the binding mode of the peroxo ligand with Mn(III), we then performed a computational study on Mn(III)–peroxo intermediate **1a**.

***End-on* $[Mn(N_3Py_2)(\eta^1\text{-}O_2)]^+$ (1a$^1$).** All the possible spin states of the *end-on* $[Mn(N_3Py_2)(\eta^1\text{-}O_2)]^+$ (**1a$^1$**) species are optimized using the B3LYP-D2 functional. Our DFT calculations reveal that the quintet state (high spin) is computed as the ground state, and this is consistent with the earlier reports on similar ligand architectures.[35] The triplet state lies at 107.6 kJ $mol^{-1}$ higher in energy, while a low-spin singlet lies at 164.4 kJ $mol^{-1}$

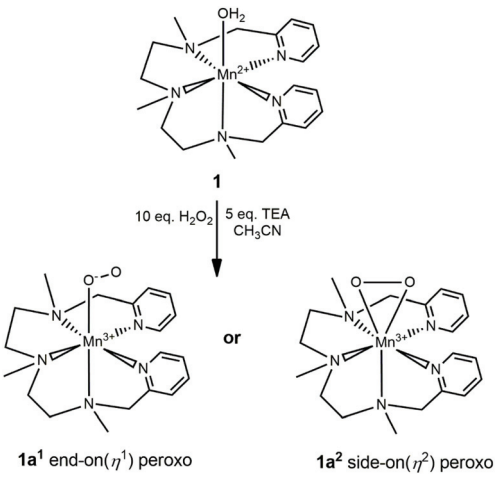


Scheme 4 Probable structure of the reactive intermediate **1a** which can exist as side-on ($\eta^2$) or end-on ($\eta^1$) peroxo.

higher in energy. The optimized structure of the high spin *end-on* $[Mn(N_3Py_2)(\eta^1\text{-}O_2)]^+$ (**1a$^1$**) species is shown in the ESI, Fig. S6a.† The Mn–O1 and O1–O2 bond lengths of the ground state of the Mn(III)–peroxo species are computed to be 2.004 Å and 1.392 Å. The Mn–N(aq) bond length is found to be 2.401 Å. The O1–Mn–N3 bond angle is computed to be 157.3°. The computed structural parameters of the quintet, triplet, and singlet spin states of the Mn(III)–peroxo species are shown in Table S2.† The ground state's spin density plot is also shown in Fig. S6b† and suggests the presence of four unpaired electrons in the d-orbital of Mn(III)–peroxo species (Table S3†).

***Side-on* $[Mn(N_3Py_2)(\eta^2\text{-}O_2)]^+$ (1a$^2$).** The possible spin states of the *side-on* $[Mn(N_3Py_2)(\eta^2\text{-}O_2)]^+$ (**1a$^2$**) species are also optimized. The B3LYP-D2 computed results show that the triplet and the singlet lie at 99.6 and 152.6 kJ mol$^{-1}$, respectively. The optimized structure of the *side-on* $[Mn(N_3Py_2)(\eta^2\text{-}O_2)]^+$ (**1a$^2$**) species is shown in Fig. S6c.† The computed Mn–O1, Mn–O2, and O1–O2 bond lengths of the ground state are 2.037 Å, 2.044 Å, and 1.443 Å. The axial Mn–N bond length is computed to be 2.458 Å. The O1–Mn–N3 and O2–Mn–N3 bond angles are found to be 154.0° and 150.3°. The computed structural parameters of *side-on* $[Mn(N_3Py_2)(\eta^2\text{-}O_2)]^+$ (**1a$^2$**) species are shown in Table S2.† The spin density plot of the ground state is shown in Fig. S6d† and the spin density data is given in Table S3.†

DFT calculations predicted that the *side-on* $[Mn(N_3Py_2)(\eta^2\text{-}O_2)]^+$ (**1a$^2$**) species is found to be the lowest in energy by 14.6 kJ mol$^{-1}$ compared with the *end-on* $[Mn(N_3Py_2)(\eta^1\text{-}O_2)]^+$ (**1a$^1$**) species. The B3LYP functional was also employed for the optimization of the structural parameter (Table S4†), which further suggests the *side-on* $[Mn(N_3Py_2)(\eta^2\text{-}O_2)]^+$ (**1a$^2$**) as the more stable intermediate than the *end-on* $[Mn(N_3Py_2)(\eta^1\text{-}O_2)]^+$ (**1a$^1$**) species. The DFT optimized structure of **1a** is shown in Fig. 4, and DFT results are in accordance with the literature report wherein *side-on* ($\eta^2$-$O_2$) binding mode is observed in Mn(III)–peroxo species bearing a pentadentate N5 ligand showing seven coordination around Mn(III).[28–31,33] In some other cases, to form the *side-on* peroxo complex, the one arm of the pentadentate ligand is free; thus, a six-coordinate Mn(III) complex is formed,[34] unlike the present case. The axial Mn–N bond length of the *side-on* $[Mn(N_3Py_2)(\eta^2\text{-}O_2)]^+$ (**1a$^2$**) species is slightly longer than that of the six-coordinate *end-on* $[Mn(N_3Py_2)(\eta^1\text{-}O_2)]^+$ (**1a$^1$**) species (Table S2†), and this is due to the presence of two ligated oxygen molecules. A significant spin density on proximal oxygen (ESI, Fig. S6d†) facilitates the reactivity of **1a**. Since **1a** is relatively stable at room temperature, our efforts are underway to grow the single crystal of **1a**.

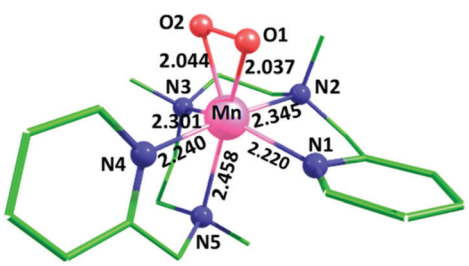


Fig. 4 DFT optimized structure of $[Mn(N_3Py_2)(O_2)]^+$ **1a**.

## Conclusions

We have described the synthesis and characterization of a new mononuclear non-heme Mn(III)peroxo species stabilized by a pentadentate $N_3Py_2$ ligand. The species is metastable at room temperature. The Mn(III)peroxo species depicts its reactivity in aldehyde deformylation on reacting with 2-PPA. The kinetics of reactions was monitored by following the decay of the peak corresponding to Mn(III)–peroxo. The activation parameters $\Delta H^{\ddagger}$ and $\Delta S^{\ddagger}$ for the aldehyde deformylation reaction were obtained from the Eyring plot and activation energy $E_a$ from the Arrhenius equation by performing the reactions at a different temperature ranging from 288 to 303 K. A KIE = 1.7 was obtained on carrying out the reaction with α-[$D_1$]-PPA. KIE = 1.7 and a positive ($\rho$) value of 3.0 suggest that the deformylation reaction proceeds by nucleophilic attack on the carbonyl group. DFT calculations were performed to provide evidence for the *side-on* binding mode of the $(O_2)^{2-}$ ligand to Mn(III).

## Conflicts of interest

There are no conflicts to declare.

## Acknowledgements

SND gratefully acknowledges the Council of Scientific and Industrial Research (CSIR), New Delhi, India (No. 01(2923)/18/EMR-II), for financial support, University Grants Commission (UGC) and Department of Science and Technology (DST), New Delhi, India, for the support to School of Chemical Sciences, Goa University, through their SAP and FIST programs. D.D.N thanks UGC, New Delhi, for SRF Fellowship (UGC-BSR). AKV acknowledges SERB, India (PDF/2016/001158). MS sincerely acknowledges the DST for the award of the DST-Inspire Faculty research grant (IFA-17-CH286). SND thanks IISER Pune for providing the ESI-MS and NMR facility.

## Notes and references

1 (*a*) P. R. O. De Montellano, *Cytochrome P450: structure, mechanism, and biochemistry*, Springer Science & Business Media, 2005; (*b*) J. Lawrence Que, W. B. Tolman, J. McCleverty and T. J. Meyer, in *Comprehensive Coordination Chemistry II: From Biology to Nanotechnology*, Elsevier, Oxford, 2004; (*c*) B. Meunier, *Biomimetic oxidations*

*catalyzed by transition metal complexes*, World Scientific, 2000.
2 E. J. Larson and V. J. Pecoraro, *Manganese redox enzymes*, VCH Publishers, New York, 1992.
3 (*a*) C. Bull, E. C. Niederhoffer, T. Yoshida and J. A. Fee, *J. Am. Chem. Soc.*, 1991, **113**, 4069–4076; (*b*) A. S. Hearn, C. Tu, H. S. Nick and D. N. Silverman, *J. Biol. Chem.*, 1999, **274**, 24457–24460.
4 J. A. Cotruvo Jr., T. A. Stich, R. D. Britt and J. Stubbe, *J. Am. Chem. Soc.*, 2013, **135**, 4027–4039.
5 W. A. Gunderson, A. I. Zatsman, J. P. Emerson, E. R. Farquhar, L. Que, J. D. Lipscomb and M. P. Hendrich, *J. Am. Chem. Soc.*, 2008, **130**, 14465–14467.
6 J. P. McEvoy and G. W. Brudvig, *Chem. Rev.*, 2006, **106**, 4455–4483.
7 J. Porta, A. Vahedi-Faridi and G. E. O. Borgstahl, *J. Mol. Biol.*, 2010, **399**, 377–384.
8 D. F. Leto and T. A. Jackson, *J. Biol. Inorg. Chem.*, 2014, **19**, 1–15.
9 R. B. VanAtta, C. E. Strouse, L. K. Hanson and J. S. Valentine, *J. Am. Chem. Soc.*, 1987, **109**, 1425–1434.
10 (*a*) N. Kitajima, H. Komatsuzaki, S. Hikichi, M. Osawa and Y. Moro-oka, *J. Am. Chem. Soc.*, 1994, **116**, 11596–11597; (*b*) U. P. Singh, A. K. Sharma, S. Hikichi, H. Komatsuzaki, Y. Moro-oka and M. Akita, *Inorg. Chim. Acta*, 2006, **359**, 4407–4411.
11 (*a*) S. Sahu and D. P. Goldberg, *J. Am. Chem. Soc.*, 2016, **138**, 11410–11428; (*b*) M. Guo, Y.-M. Lee, R. Gupta, M. S. Seo, T. Ohta, H.-H. Wang, H.-Y. Liu, S. N. Dhuri, R. Sarangi, S. Fukuzumi and W. Nam, *J. Am. Chem. Soc.*, 2017, **139**, 15858–15867; (*c*) D. B. Rice, A. A. Massie and T. A. Jackson, *Acc. Chem. Res.*, 2017, **50**, 2706–2717.
12 (*a*) S. Groni, G. Blain, R. Guillot, C. Policar and E. Anxolabéhère-Mallart, *Inorg. Chem.*, 2007, **46**, 1951–1953; (*b*) H. E. Colmer, A. W. Howcroft and T. A. Jackson, *Inorg. Chem.*, 2016, **55**, 2055–2069; (*c*) R. A. Geiger, S. Chattopadhyay, V. W. Day and T. A. Jackson, *J. Am. Chem. Soc.*, 2010, **132**, 2821–2831; (*d*) H. E. Colmer, R. A. Geiger, D. F. Leto, G. B. Wijeratne, V. W. Day and T. A. Jackson, *Dalton Trans.*, 2014, **43**, 17949–17963; (*e*) R. A. Geiger, S. Chattopadhyay, V. W. Day and T. A. Jackson, *Dalton Trans.*, 2011, **40**, 1707–1715.
13 (*a*) H. Kang, J. Cho, K.-B. Cho, T. Nomura, T. Ogura and W. Nam, *Chem. – Eur. J.*, 2013, **19**, 14119–14125; (*b*) M. S. Seo, J. Y. Kim, J. Annaraj, Y. Kim, Y. M. Lee, S. J. Kim, J. Kim and W. Nam, *Angew. Chem., Int. Ed.*, 2007, **46**, 377–380; (*c*) J. Annaraj, J. Cho, Y.-M. Lee, S. Y. Kim, R. Latifi, S. P. de Visser and W. Nam, *Angew. Chem., Int. Ed.*, 2009, **48**, 4150–4153; (*d*) R. A. Geiger, G. B. Wijeratne, V. W. Day and T. A. Jackson, *Eur. J. Inorg. Chem.*, 2012, **2012**, 1598–1608; (*e*) J. Du, D. Xu, C. Zhang, C. Xia, Y. Wang and W. Sun, *Dalton Trans.*, 2016, **45**, 10131–10135; (*f*) P. Barman, P. Upadhyay, A. S. Faponle, J. Kumar, S. S. Nag, D. Kumar, C. V. Sastri and S. P. de Visser, *Angew. Chem., Int. Ed.*, 2016, **55**, 11091–11095; (*g*) F. G. Cantú Reinhard, P. Barman, G. Mukherjee, J. Kumar, D. Kumar, D. Kumar, C. V. Sastri and S. P. de Visser, *J. Am. Chem. Soc.*, 2017, **139**, 18328–18338; (*h*) J. Du, C. Miao, C. Xia and W. Sun, *Chin. Chem. Lett.*, 2018, **29**, 1869–1871; (*i*) P. Barman, F. G. Cantú Reinhard, U. K. Bagha, D. Kumar, C. V. Sastri and S. P. de Visser, *Angew. Chem., Int. Ed.*, 2019, **58**, 10639–10643; (*j*) R. A. Geiger, D. F. Leto, S. Chattopadhyay, P. Dorlet, E. Anxolabéhère-Mallart and T. A. Jackson, *Inorg. Chem.*, 2011, **50**, 10190–10203.
14 S. El Ghachtouli, H. Y. Vincent Ching, B. Lassalle-Kaiser, R. Guillot, D. F. Leto, S. Chattopadhyay, T. A. Jackson, P. Dorlet and E. Anxolabéhère-Mallart, *Chem. Commun.*, 2013, **49**, 5696–5698.
15 (*a*) R. L. Shook, W. A. Gunderson, J. Greaves, J. W. Ziller, M. P. Hendrich and A. S. Borovik, *J. Am. Chem. Soc.*, 2008, **130**, 8888–8889; (*b*) R. L. Shook and A. S. Borovik, *Inorg. Chem.*, 2010, **49**, 3646–3660; (*c*) M. Sankaralingam, Y.-M. Lee, S. H. Jeon, M. S. Seo, K.-B. Cho and W. Nam, *Chem. Commun.*, 2018, **54**, 1209–1212.
16 (*a*) D. F. Leto, R. Ingram, V. W. Day and T. A. Jackson, *Chem. Commun.*, 2013, **49**, 5378–5380; (*b*) M. Sankaralingam, S. H. Jeon, Y.-M. Lee, M. S. Seo, K. Ohkubo, S. Fukuzumi and W. Nam, *Dalton Trans.*, 2016, **45**, 376–383.
17 (*a*) X. Wu, M. S. Seo, K. M. Davis, Y.-M. Lee, J. Chen, K.-B. Cho, Y. N. Pushkar and W. Nam, *J. Am. Chem. Soc.*, 2011, **133**, 20088–20091; (*b*) J. Chen, Y.-M. Lee, K. M. Davis, X. Wu, M. S. Seo, K.-B. Cho, H. Yoon, Y. J. Park, S. Fukuzumi, Y. N. Pushkar and W. Nam, *J. Am. Chem. Soc.*, 2013, **135**, 6388–6391.
18 D. D. Narulkar, K. Devulapally, A. K. Undrajavarapu, S. N. Dhuri, V. M. Dhavale, A. K. Vardhaman and L. Giribabu, *Sustainable Energy Fuels*, 2020, **4**, 2656–2660.
19 D. D. Narulkar, A. K. Srivastava, R. J. Butcher, K. M. Ansy and S. N. Dhuri, *Inorg. Chim. Acta*, 2017, **467**, 405–414.
20 (*a*) C. R. Goldsmith, R. T. Jonas and T. D. P. Stack, *J. Am. Chem. Soc.*, 2002, **124**, 83–96; (*b*) C. Arunkumar, Y.-M. Lee, J. Y. Lee, S. Fukuzumi and W. Nam, *Chem. – Eur. J.*, 2009, **15**, 11482–11489; (*c*) S. N. Dhuri, Y.-M. Lee, M. S. Seo, J. Cho, D. D. Narulkar, S. Fukuzumi and W. Nam, *Dalton Trans.*, 2015, **44**, 7634–7642.
21 M. Frisch, G. Trucks, H. B. Schlegel, G. E. Scuseria, M. A. Robb, J. R. Cheeseman, G. Scalmani, V. Barone, B. Mennucci, G. Petersson, H. Nakatsuji, M. Caricato, X. Li, H. P. Hratchian, A. F. Izmaylov, J. Bloino, G. Zheng, J. L. Sonnernberg, M. Hada, M. Ehara, K. Toyata, R. Fukuda, J. Hasegawa, M. Ishida, T. Nakajima, Y. Honda, O. Kitao, H. Nakai, T. Vreven, J. A. Montgonery Jr., J. E. Paralta, F. Ogliaro, M. Bearpark, J. J. Heyd, E. Brothers, K. N. Kudin, V. N. Staroverov, R. Kobayashi, J. Normand, K. Raghavachari, A. Rendell, J. C. Burant, S. S. Iyengar, J. Tomasi, M. Cossi, N. Rega, J. M. Millam, M. Klene, J. E. Khox, J. B. Cross, V. Bakken, C. Adamo, J. Jaramillo, R. Gomperts, R. E. Stratmann, O. Yazyev, A. J. Austin, R. Cammi, C. Pomelli, J. W. Ochterski, R. L. Martin, K. Morokuma, V. G. Zakrzewski, G. A. Voth, P. Salvador, J. J. Dannenberg, S. Dapprich, A. D. Daniels, O. Farkas,

 

J. B. Foresman, J. V. Ortiz, J. Cioslowski and D. J. Fox, *Gaussian 09 (Revision A.1)*, Gaussion, Inc., Wallingford CT, 2009.

22 A. Ansari, A. Kaushik and G. Rajaraman, *J. Am. Chem. Soc.*, 2013, **135**, 4235–4249.

23 S. Grimme, *J. Comput. Chem.*, 2006, **27**, 1787–1799.

24 (*a*) T. H. Dunning Jr. and P. J. Hay, in *J Methods of Electronic Structure Theory*, ed. H. F. Schaefer III, Plenum, New York, 1976, pp. 1; (*b*) P. J. Hay and W. R. Wadt, *J. Chem. Phys.*, 1985, **82**, 270–283; (*c*) W. R. Wadt and P. J. Hay, *J. Chem. Phys.*, 1985, **82**, 284–298; (*d*) P. J. Hay and W. R. Wadt, *J. Chem. Phys.*, 1985, **82**, 299–310.

25 R. Ditchfield, W. J. Hehre and J. A. Pople, *J. Chem. Phys.*, 1971, **54**, 724–728.

26 (*a*) A. Schäfer, H. Horn and R. Ahlrichs, *J. Chem. Phys.*, 1992, **97**, 2571–2577; (*b*) A. Schäfer, C. Huber and R. Ahlrichs, *J. Chem. Phys.*, 1994, **100**, 5829–5835.

27 N. Saravanan, M. Sankaralingam and M. Palaniandavar, *RSC Adv.*, 2014, **4**, 12000–12011.

28 (*a*) D. F. Evans, *J. Chem. Soc.*, 1959, 2003–2005, DOI: 10.1039/jr9590002003; (*b*) S. Das, Kulbir, S. Ghosh, S. C. Sahoo and P. Kumar, *Chem. Sci.*, 2020, **11**, 5037–5042; (*c*) M. Yenuganti, S. Das, Kulbir, S. Ghosh, P. Bhardwaj, S. S. Pawar, S. C. Sahoo and P. Kumar, *Inorg. Chem. Front.*, 2020, **7**, 4872–4882.

29 (*a*) J. Cho, R. Sarangi, H. Y. Kang, J. Y. Lee, M. Kubo, T. Ogura, E. I. Solomon and W. Nam, *J. Am. Chem. Soc.*, 2010, **132**, 16977–16986; (*b*) J. Cho, R. Sarangi, J. Annaraj, S. Y. Kim, M. Kubo, T. Ogura, E. I. Solomon and W. Nam, *Nat. Chem.*, 2009, **1**, 568–572; (*c*) Y. Jo, J. Annaraj, M. S. Seo, Y.-M. Lee, S. Y. Kim, J. Cho and W. Nam, *J. Inorg. Biochem.*, 2008, **102**, 2155–2159.

30 M. Akhtar, D. Corina, S. Miller, A. Z. Shyadehi and J. N. Wright, *Biochemistry*, 1994, **33**, 4410–4418.

31 S. H. Bae, X.-X. Li, M. S. Seo, Y.-M. Lee, S. Fukuzumi and W. Nam, *J. Am. Chem. Soc.*, 2019, **141**, 7675–7679.

32 W. D. Bailey, N. L. Gagnon, C. E. Elwell, A. C. Cramblitt, C. J. Bouchey and W. B. Tolman, *Inorg. Chem.*, 2019, **58**, 4706–4711.

33 (*a*) D. L. Wertz and J. S. Valentine, in *Metal-Oxo and Metal-Peroxo Species in Catalytic Oxidations*, ed. B. Meunier, Springer Berlin Heidelberg, Berlin, Heidelberg, 2000, pp. 37–60, DOI: 10.1007/3-540-46592-8_2; (*b*) J. Annaraj, Y. Suh, M. S. Seo, S. O. Kim and W. Nam, *Chem. Commun.*, 2005, 4529–4531; (*c*) X. Hu, I. Castro-Rodriguez and K. Meyer, *J. Am. Chem. Soc.*, 2004, **126**, 13464–13473; (*d*) J. Cho, R. Sarangi and W. Nam, *Acc. Chem. Res.*, 2012, **45**, 1321–1330; (*e*) J. Cho, H. Y. Kang, L. V. Liu, R. Sarangi, E. I. Solomon and W. Nam, *Chem. Sci.*, 2013, **4**, 1502–1508.

34 J. Kim, B. Shin, H. Kim, J. Lee, J. Kang, S. Yanagisawa, T. Ogura, H. Masuda, T. Ozawa and J. Cho, *Inorg. Chem.*, 2015, **54**, 6176–6183.

35 A. Ansari, P. Jayapal and G. Rajaraman, *Angew. Chem., Int. Ed.*, 2015, **54**, 564–568.